The 4-Day Wave and Transport of *UARS* Tracers in the Austral Polar Vortex

G. L. MANNEY

Jet Propulsion Laboratory, California Institute of Technology, Pasadena, California

Y. J. ORSOLINI

Centre National de Recherches Météorologiques, Toulouse, France

H. C. PUMPHREY

Department of Meteorology, University of Edinburgh, Edinburgh, United Kingdom

A. E. ROCHE

Lockheed Martin Palo Alto Research Laboratory, Palo Alto, California

(Manuscript received 12 August 1997, in final form 26 February 1998)

ABSTRACT

Upper Atmosphere Research Satellite tracer data and isentropic transport calculations using U.K. Meteorological Office winds initialized with these data show evidence of eastward-traveling waves in the polar upper stratosphere in late austral winter 1992. Microwave Limb Sounder (MLS) H_2O from prototype iterative retrievals shows a 4-day wave signal at levels from ~1.5 to 0.1 hPa; a 4-day wave signal was not obvious in production retrievals of MLS H_2O. At 1800 K, the 4-day wave signal in MLS H_2O has a double-peaked structure in latitude, which is reproduced in isentropic transport calculations. The time evolution, amplitude, and phase of the 4-day wave in the transport calculations agree well with observations at high latitudes; the position and shape of the polar vortex and of H_2O drawn up around the vortex are reproduced by the transport calculations. Spectral analyses of the Cryogen Limb Array Etalon Spectrometer (CLAES) CH_4 are dominated by more slowly eastward-moving waves (~6–10 days), but a weak 4-day wave signature is also present between ~1.5 and 4 hPa. Transport calculations initialized with CH_4 show similar eastward-traveling signals, good agreement with the phase of the observed signals, and overall agreement with the observed position of the vortex. The qualitative success of the transport calculations in reproducing the phase and overall time evolution of high-latitude eastward-traveling waves in the polar upper stratosphere indicates that the winds used for the transport calculations are generally reliable, and that the eastward-traveling waves identified in the MLS H_2O and CLAES CH_4 originate to a large extent from horizontal transport processes. Examination of the vertical structure of potential vorticity shows periods when at the highest levels studied (around 1800 K), the 4-day wave is responsible for the main motion of the vortex, whereas at lower levels (at and below ~1400 K) the vortex motion is characterized by a slower eastward progression, and the 4-day wave signal contributes to motions that are confined inside the vortex.

1. Introduction

Many observational and theoretical studies have focused on the 4-day eastward moving wave in the polar winter upper stratosphere and mesosphere. Allen et al. (1997) give a review of such studies; the 4-day wave is characterized by waves of zonal wavenumber 1 through at least 4, moving with the same phase speed, such that the wave 1 period is near 4 days. The 4-day wave is observed in both hemispheres, although it is stronger in the Southern Hemisphere (e.g., Venne and Stanford 1982). Theoretical studies (Manney and Randel 1993, and references therein) show that the observed characteristics of the 4-day wave are consistent with it originating through instability of the polar night jet in the upper stratosphere and lower mesosphere; many observed episodes of 4-day wave growth are consistent with primarily barotropic instability (e.g., little vertical phase tilt, poleward momentum flux), although some show evidence of the importance of both barotropic and baroclinic effects (e.g., equatorward momentum and heat flux, phase tilt with height) (e.g., Manney 1991; Randel and Lait 1991; Allen et al. 1997 and references therein).

Bowman and Chen (1994) and Orsolini and Simon (1995) studied the nonlinear evolution of barotropically

Corresponding author address: Dr. Gloria L. Manney, Jet Propulsion Laboratory, California Institute of Technology, Mail Stop 183-701, 4800 Oak Grove Dr. Pasadena, CA 91109.
E-mail: manney@mls.jpl.nasa.gov

unstable modes including the 4-day wave and transport associated with these using idealized models. Bowman and Chen found that unstable modes poleward of the polar night jet produced weak mixing that was entirely confined to the vortex. Orsolini and Simon found extensive mixing within the vortex during wave growth, and mixing between the vortex and its edge during wave decay.

Allen et al. (1997) presented evidence of the 4-day wave in temperature, geopotential height, and ozone data from the *Upper Atmosphere Research Satellite* (*UARS*) Microwave Limb Sounder (MLS) in the 1992 and 1993 late Southern Hemisphere (SH) winters, in the upper stratosphere and lower mesosphere. Other eastward moving wave features have also been identified in MLS temperature and ozone data in the 1992 late SH winter in the upper stratosphere (Fishbein et al. 1993), and Lahoz et al. (1996a) examined the evolution of the middle-stratospheric polar vortex during this period.

In the SH late winter of 1992, several other fields are available from *UARS* instruments, in particular water vapor (H_2O) from MLS and methane (CH_4) from the Cryogen Limb Array Etalon Spectrometer (CLAES). At levels below ~65 km, the chemical lifetimes of both H_2O and CH_4 are months to years (e.g., Brasseur and Solomon 1986), so their evolution on timescales of days and weeks should be controlled primarily by transport. In the following we examine these fields for evidence of eastward traveling waves, in particular, the 4-day wave. We use MLS H_2O, CLAES CH_4, and idealized tracers to initialize isentropic transport calculations, allowing qualitative comparison of the calculated wave signatures due to horizontal transport processes with the observed 4-day wave signatures.

2. Data and analysis

The MLS Version 3 H_2O data and validation are described by Lahoz et al. (1996b). Both these and the version 4 production retrievals of H_2O showed puzzling behavior in the polar middle and upper stratosphere during winter periods including the late winter 1992 period that we are interested in here (e.g., Manney et al. 1995); this behavior appeared inconsistent with the expectation that the evolution of H_2O in the middle and upper stratosphere is driven primarily by transport. The production retrievals of MLS H_2O have several other known flaws. Some are due to the fact that the production retrieval is not iterative—this problem is worst in the lower stratosphere where the radiative transfer is most nonlinear. Some are caused by problems modeling the instrument and the atmosphere; the worst of these are due to our imperfect knowledge of the pressure broadening and shifting of the spectral lines and the sideband ratios of the instrument—these problems are present throughout the useful vertical range. Also, the production retrieval is done on a grid with a vertical spacing of 5.3 km, but the instrument is capable of better vertical resolution than this, particularly in the midstratosphere. During late winter, the H_2O mixing ratio peak is in the upper stratosphere, and is narrow, with strong vertical H_2O gradients above and below (see, e.g., Fig. 2 below); in this situation, the low vertical resolution may be an important factor in the failure of the production retrievals to show a consistent picture of H_2O transport in the polar upper stratosphere.

Recently, a prototype iterative retrieval has been developed at the University of Edinburgh's Department of Meteorology, similar to algorithms scheduled for the next version of production processing. This retrieval applies the optimal estimation equation once and then relinearizes about the result before applying it again; the process is repeated until a convergence criterion is met. The iterative retrievals are described in more detail by Pumphrey (1998). The retrieved profiles are on the standard pressure grid for *UARS* ''L3'' files; this has a spacing of ~2.6 km, twice as fine as the grid used for MLS Version 3 and 4 retrievals. The vertical resolution of the product from the prototype retrievals is better in the middle stratosphere than the ~5 km MLS Version 4 grid, but not quite as good as the 2.6 km of the L3 grid; above ~1 mb the vertical resolution is rather worse, on the order of 6 or 7 km. Examination of the overall time evolution of H_2O retrieved this way for 14 August through 19 September 1992 shows behavior that appears more consistent with transport processes than the earlier retrievals. It is these H_2O data that we focus on here. Single profile precision for these data is estimated to be ~0.15–0.35 ppmv between 10 and 0.1 hPa, with accuracy of ~0.7–0.9 ppmv.

We have also examined CLAES Version 7 CH_4 data, described by Roche et al. (1996); these have random errors of ~0.05–0.08 ppmv, and a systematic error of ~15%, with CLAES biased high with respect to correlative data. CLAES Version 8 CH_4 data are also available, but exhibit larger biases than version 7 CH_4 data, resulting from known problems in the version 8 retrieval algorithm. Analyses like those shown here using Version 8 CH_4 data show very similar results. Although CLAES in principle also observed H_2O, scientifically useful retrievals of CLAES H_2O are not yet available.

UARS data are interpolated to isentropic surfaces using temperatures from the U.K. Meteorological Office (UKMO) troposphere–stratosphere data assimilation system (Swinbank and O'Neill 1994) for comparison with isentropic transport calculations. Those spectral analyses that are being compared with transport calculations are performed using these interpolated fields. *UARS* data are provided in daily ''L3AT'' files, comprising profiles at equal time intervals along the orbit tracks, so that the alongtrack spacing is ~400 km. Once daily (1200 UTC) H_2O and CH_4 data on a 4° lat by 5° long grid were obtained from these using a Fourier analysis procedure that separates longitude and time variations (Elson and Froidevaux 1993). Since there are ~15 orbits per day and the orbit tracks become more

zonal and more closely spaced near the high-latitude turnaround points, the actual sampling by the *UARS* instruments is better than this grid spacing at high latitudes, and the longitudinal sampling is considerably worse than this at lower latitudes. The splotchy appearance in midlatitudes of the maps from observed data shown later is due at least in part to this sampling pattern. An additional complication in the spectral analysis of CH_4 is that CLAES data in the region of interest are missing for many orbits on 2 days (27 August and 1 September) during the period of study. The gridding procedure described above interpolates over missing data to produce complete gridded fields on each day. However, we have less confidence in the details of the fields on those days when the majority of the data were missing, especially since rapid changes in the flow are occurring during the time period being studied.

The spectral analysis presented here uses the same methods described by Manney (1991), who followed the methods described in more detail by Venne and Stanford (1982). For comparison with the transport calculations, we are using 24-day time series; for these shorter time series, we use an 8-day spectral window. As in Manney (1991), we present plots of the ratio of eastward moving variance to noise variance (ES/N), large values of which indicate that the wave feature could be detected in the presence of noise. The advantage of this type of display is that it isolates those signals that are significant; the disadvantage is that it does not show the absolute amplitude of the features or exact details of their spatial structure. Since we are primarily interested in the 4-day wave (part of a quasi-nondispersive feature, only the wave 1 component of which can be reliably detected in once daily data), and since wavenumber 1 features are dominant in the middle and upper stratosphere at this time (e.g., Fishbein et al. 1993), we focus here on wave 1. Figure 1 shows the ES/N at 1800 K (~1–1.5 hPa) for analyses of UKMO temperatures and version 4 MLS ozone. Although displayed differently, these results are in good agreement with those from MLS temperatures and version 3 MLS ozone shown by Allen et al. (1997). To show information on phase, amplitude, and details of spatial structure of the wave motions, we present filtered data in time–longitude (Hovmöller) plots and maps. Filtering is done in the frequency domain, as described by Manney (1991). Comparison of Hovmöller plots of the 4-day wave in UKMO temperatures shows excellent agreement in 4-day wave amplitude and evolution with that shown by Allen et al. (1997). We have also done spectral analyses of UKMO winds and potential vorticity (PV) calculated from the UKMO data and transport calculations initialized with UKMO PV.

The transport code is described by Orsolini (1995); the ability of this model to simulate high-resolution tracer fields and small-scale structure such as filamentation in those fields has previously been demonstrated (e.g., Orsolini et al. 1997, and references therein). It is used

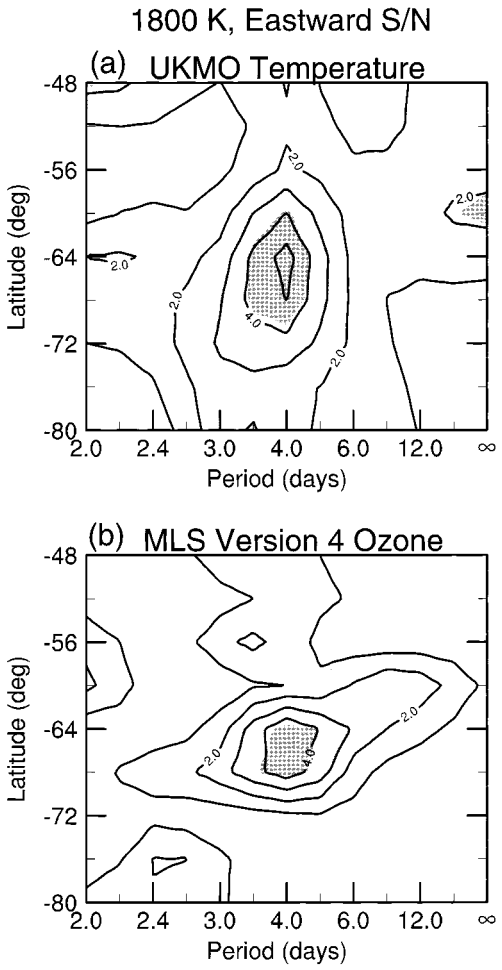

FIG. 1. Eastward moving signal-to-noise ratio (the ratio of eastward moving variance to noise variance, ES/N) from 24-day time series of (a) UKMO temperature and (b) version 4 MLS ozone beginning on 14 Aug 1992, both interpolated to the 1800 K isentropic surface. The light and dark shading shows the coherence squared at the 95% and 99% confidence levels, respectively.

here on a Gaussian T106 grid, giving ~1.125° resolution, and is run on individual isentropic surfaces that are of interest. The advecting winds are from the UKMO analyses, interpolated to the appropriate isentropic surfaces and the model grid. Transport calculations using *UARS* data were initialized with the gridded fields described above. Inconsistency between the tracer fields used for initialization and the advecting winds (resulting from inaccuracies in both datasets) may lead to a period of tracer adjustment in the first few days of the transport model run (e.g., Lary et al. 1995). In addition, since the calculations are isentropic and since, in the polar middle and upper stratosphere at this time, diabatic descent rates are relatively large (e.g., Manney et al. 1994), we do not expect to quantitatively reproduce the observed fields with the transport calculations, but only to examine the ability of these calculations to reproduce the

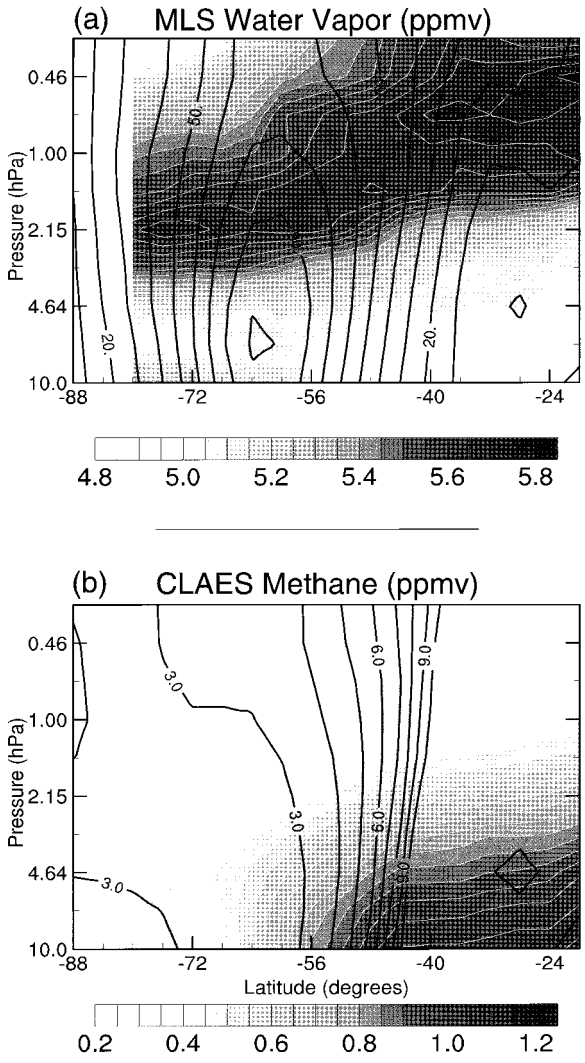

FIG. 2. Zonal-mean, time-mean (a) MLS H_2O and (b) CLAES CH_4 for 28–31 Aug 1992, with contours of (a) UKMO zonal wind and (b) ''wind period'' calculated from UKMO zonal wind overlaid.

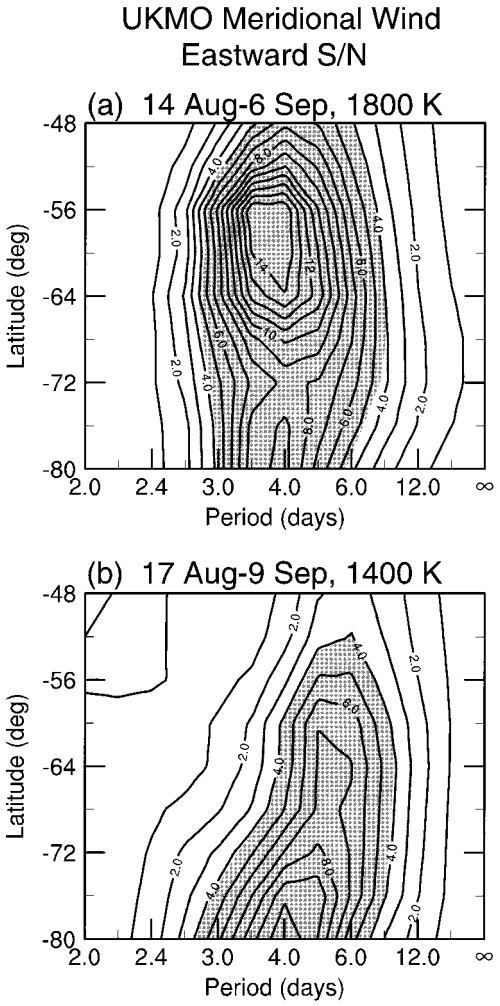

FIG. 3. ES/N for 24-day time series of UKMO meridional wind (a) at 1800 K beginning on 14 Aug 1992 and (b) at 1400 K beginning on 17 Aug 1992. Shading is as in Fig. 1.

general features of the transport of the tracers by traveling planetary scale waves.

Transport calculations and spectral analyses are done for 24-day periods, starting on 14 August 1992 for calculations with MLS H_2O, and on 17 August 1992 for CLAES CH_4; each starting date is the first complete day on which data from that instrument are available at high southern latitudes in that observing period. For spectral analyses and Hovmöller plots, we have sampled the output of the transport calculations once daily at 1200 UTC, consistent with the gridded observed tracer fields.

3. Results

a. Overview

To first order, assuming linear wave theory, the amplitude of a wave in a passive tracer transported by horizontal motions goes as

$$\mu'^2 \sim \frac{1}{k^2(\overline{u} - c)^2}\left[\left(\frac{\partial \overline{\mu}}{\partial y}\right)^2 v'^2\right],$$

where μ' and v' are the amplitudes of sinusoidally varying wave components of mixing ratio and meridional velocity, respectively, with wavenumber k and phase speed c [see, e.g., Allen et al. (1997), Eqs. (8) and (9)]. Thus, we would expect to see waves amplify in the tracer field where $(\overline{u} - c)$ is small, the amplitude of the perturbation in the meridional velocity is large, and the zonal-mean tracer mixing ratio exhibits significant meridional gradients. Figure 2 shows cross sections of zonal-mean H_2O and CH_4 mixing ratios with overlaid contours of zonal-mean wind and ''wind period'' (the time for a parcel moving at the zonal-mean wind speed to progress completely around a latitude circle), respectively, averaged over 4 days near the middle of the time period we are considering. In late winter the peak in MLS H_2O in the polar regions is near 2 hPa, and H_2O

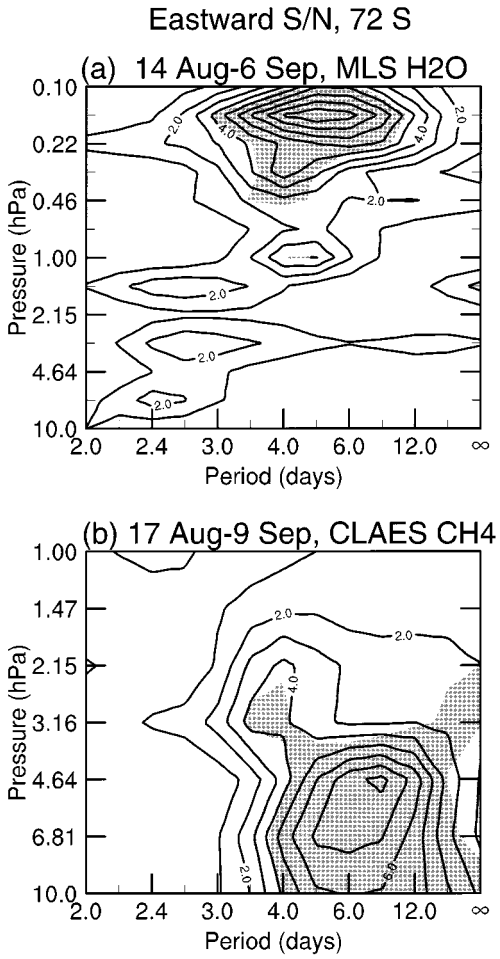

FIG. 4. ES/N at 72°S for 24-day time series of (a) MLS H_2O beginning on 14 Aug 1992 and (b) CLAES CH_4 beginning on 17 Aug 1992. Shading is as in Fig. 1.

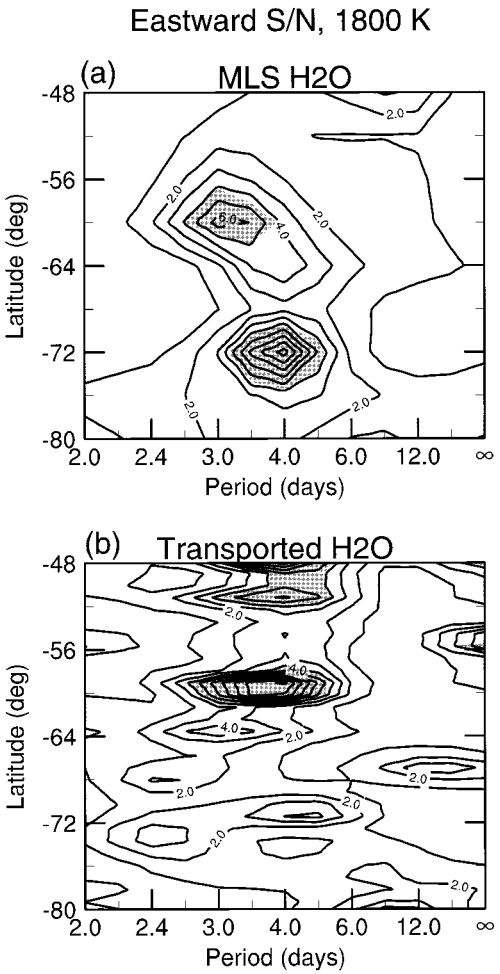

FIG. 5. ES/N at 1800 K for 24-day time series beginning on 14 Aug 1992 of (a) observed MLS H_2O and (b) H_2O from a transport calculation initialized with MLS H_2O on 14 Aug 1992. Shading is as in Fig. 1.

shows significant horizontal tracer gradients at high latitudes only above about 1.5 hPa. In contrast, CLAES CH_4 shows strong horizontal gradients at high latitudes only below about 2 hPa. Wherever the wind period shown in Fig. 2b is near the wave 1 period, $(\overline{u} - c)$ will be small. For the 4-day wave, this includes a broad region poleward of ~50°S. During the period of study, the zonal-mean winds are changing rapidly. A similar average over 2–5 September shows a region of 3–6 day wind periods that is considerably narrower and shifted 5–10° poleward of that shown in Fig. 2b. Thus the conditions necessary for observable tracer transport by wave motions vary considerably, even during the short period of study. Figure 3 shows ES/N for UKMO meridional winds at 1800 and 1400 K, for time series beginning on 14 August and 17 August, respectively, indicating a strong signal with a period near 4 days and a double-peaked structure in latitude at 1800 K and a signal at 1400 K with a period near 4 days at high latitudes and somewhat longer periods (near 5–7 days) at ~50°–60°S.

Figure 4 shows ES/N for H_2O and CH_4 at 72°S as a function of pressure, for time series beginning on 14 August and 17 August, respectively. As suggested by the above general arguments, H_2O shows a signal with a period near 4 days at levels above about 1.5 hPa, extending well into the mesosphere, and CH_4 shows a signal with a period near 4 days at about 3 hPa, and longer period (5–10 days) signals below. In the following, we compare wave motions in H_2O and CH_4 with isentropic transport calculations. Although UKMO temperatures, which themselves include a 4-day wave signal, are used to interpolate the *UARS* data to isentropic surfaces, Fig. 4 demonstrates clearly that the wave motions discussed below are, in fact, present in the tracer data themselves.

b. Water vapor

The UKMO data are available only up to 0.316 hPa and become somewhat noisy in the top few levels for

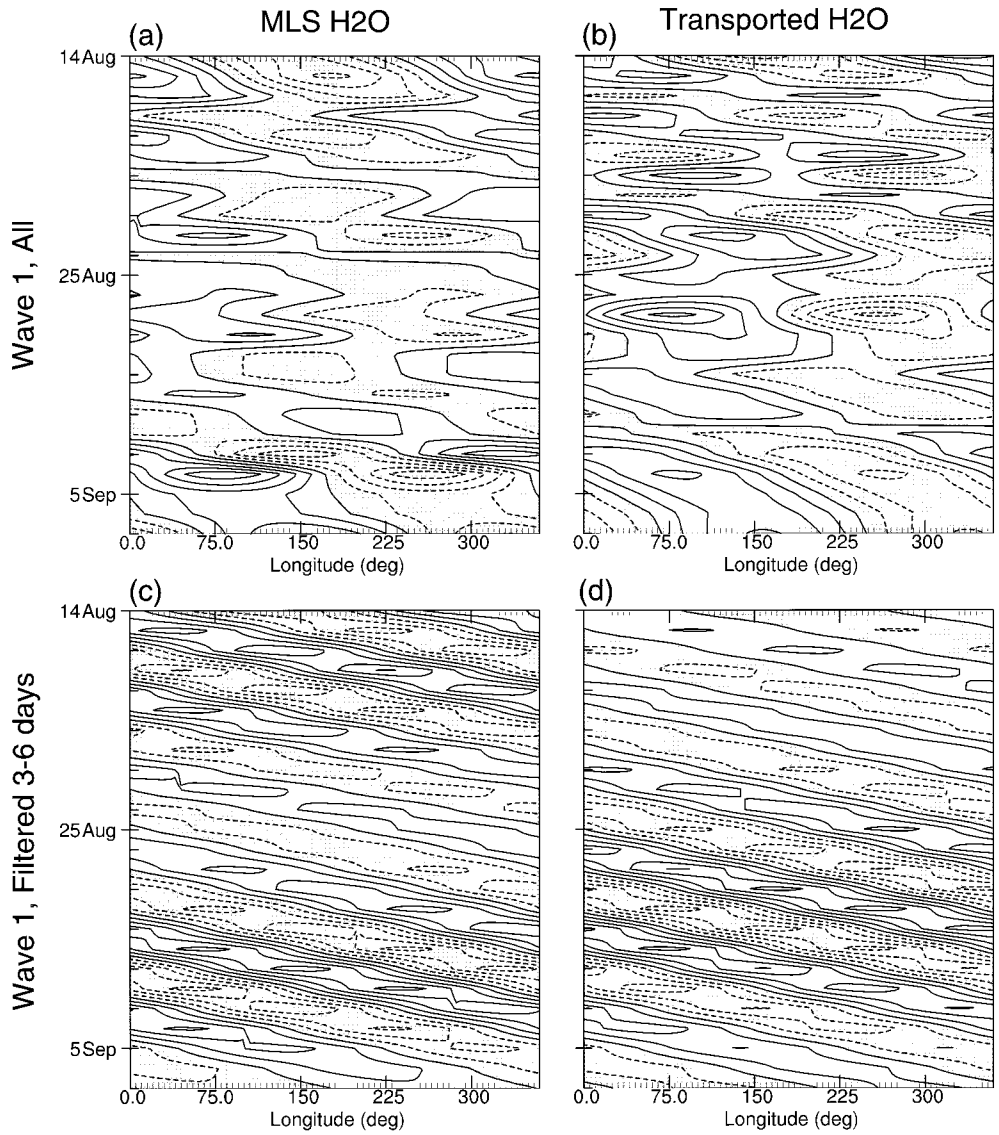

FIG. 6. Time–longitude (Hovmöller) plots at 72°S of wave 1 in H_2O from (a) and (c) MLS observations and (b) and (d) transport calculations, showing (a) and (b) total wave 1 field and (c) and (d) wave 1 filtered for 2.9–6.4-day periods. Contour interval in (a) and (b) is 0.05 ppmv; in (c) and (d), 0.016 ppmv. Negative values are shaded.

which they are available, above about 1 hPa (Swinbank and O'Neill 1994). We therefore chose to run transport calculations initialized with H_2O at 1800 K (~1.5 hPa at 80°S to 1 hPa at 50°S), which is the highest level for which we feel the winds are sufficiently reliable, and the temperatures reliable for interpolating the tracer data to isentropic surfaces. Figure 5 compares ES/N for MLS H_2O at 1800 K with that for a transport calculation initialized with MLS H_2O on 14 August 1992. The observed 4-day wave signal shows strong peaks near 72°S and 60°S. Although the signal from the transport calculation shows much more latitudinal structure (recall that the transport calculation has ~1.125° resolution, as opposed to 4° for the gridded MLS data), there are distinct peaks near 72° and 60°S with periods near to those seen in the observations. At lower latitudes, the observed and calculated signals do not agree well, and the calculations show some additional weaker features (e.g., at ~74°S, 2.4 d and 68°S, 12 d) that are not apparent in the observations. A similar transport calculation was done for this period for an idealized tracer (''PV tracer'') whose initial mixing ratio was the UKMO PV at 1800 K on 14 August 1992; spectral analyses of UKMO PV and transported PV tracer at 1800 K show ES/N patterns very similar to those seen in H_2O, with peaks of about 4-day periods at ~72°S and 60°S.

Figure 6 compares time–longitude (Hovmöller) plots of wave 1, and wave 1 filtered for 2.9–6.4 d periods,

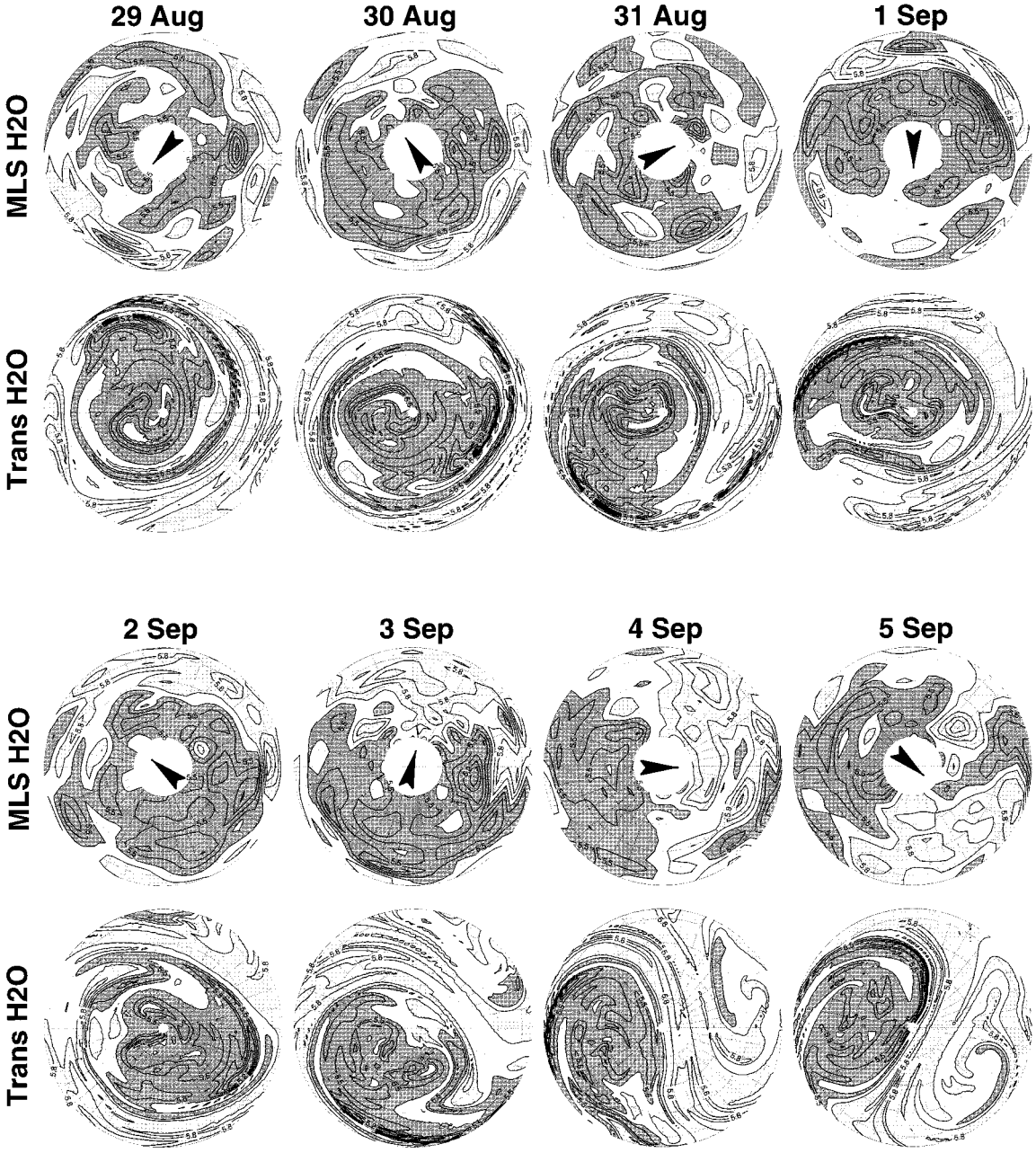

FIG. 7. Maps of H_2O (ppmv) at 1800 K for 29 Aug–5 Sep 1992 from MLS observations (top) and transport calculations (bottom). The projection is orthographic, with 0° long at the top and 90°E to the right; the outer edge is at 46°S, with dashed lines every 10° lat and long. Contour interval is 0.1 ppmv, with dark shading from 4.8 to 5.6 ppmv and light shading from 5.7 to 6.5 ppmv.

for observed and transported H_2O at 1800 K. The overall agreement between the observed and calculated fields is variable near the beginning of the transport calculation, possibly due to tracer adjustment in the calculation (e.g., Lary et al. 1995). After about 25 August 1992, the observed and calculated wave 1 phases agree well, and a fast eastward-moving feature is readily apparent in the full wave 1 fields around 30 August–3 September 1992, with a more slowly eastward-moving feature amplifying after that time. Comparison of amplitudes in the filtered and unfiltered plots indicates that the 4-day wave represents nearly all of the 72°S wave 1 signal during 31 August–2 September. The filtered fields show good agreement in the 4-day wave features, in that the phase is nearly identical for each, and the time evolution is similar (although amplification begins slightly earlier in the transport model), with maximum amplitudes between about 25 and 30 August 1992, after which time amplitudes decrease slowly. The maximum amplitudes seen in the transport calculation are similar to those

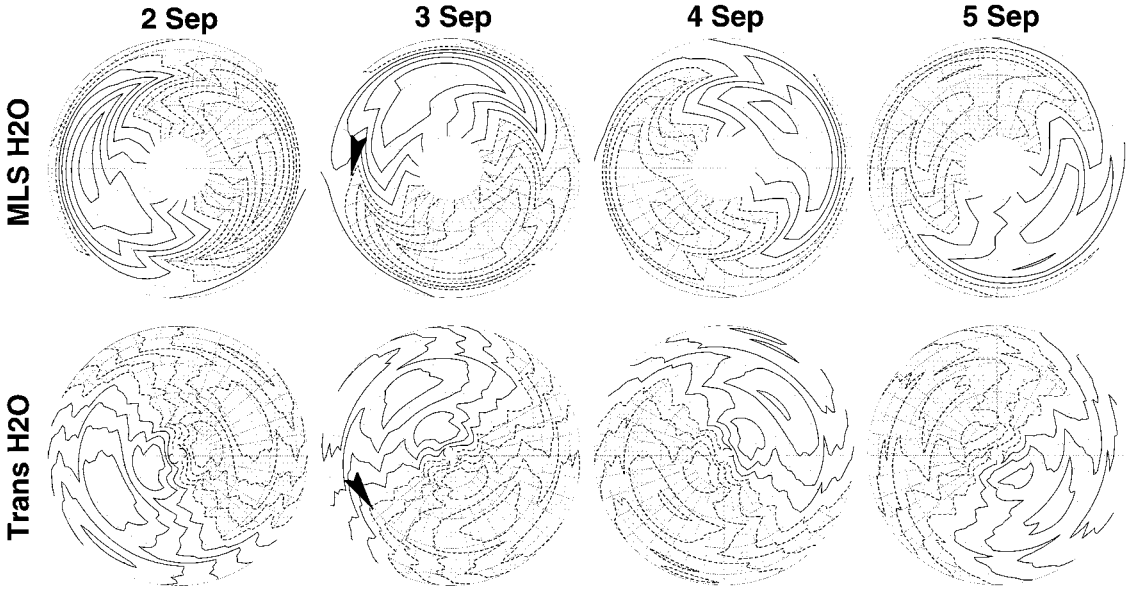

FIG. 8. Maps of wave 1 in H_2O (ppmv) filtered for 2.9–6.4-day periods at 1800 K for 2–5 Sep 1992 (the last 4 days shown in Fig. 7) from MLS observations (top) and transport calculations (bottom). Layout is as in Fig. 7. Negative values are shaded.

observed. Comparison to Hovmöller plots of the 4-day wave in temperature (e.g., Allen et al. 1997) and meridional velocity shows that the 4-day wave in H_2O is 90° out of phase with the perturbation in meridional velocity and in phase with the temperature perturbation; this is consistent with the relationships found by Hartmann and Garcia (1979) for transport by planetary-scale waves of a dynamically controlled tracer in a quasi-geostrophic model.

Figure 7 shows an eight-day sequence of maps of observed and transported H_2O fields at 1800 K, for 29 August–5 September. Around 5 September, slowly moving and quasi-stationary wave 1 components amplify and are in phase, leading to a very large total wave 1 amplitude (Fishbein et al. 1993). As was apparent at 72°S in Fig. 6, the 4-day wave is a dominant high-latitude feature at this time. This is shown in the orientation (defined as the meridian pointing most nearly from low H_2O on one side of the pole to high H_2O on the other, shown approximately by arrows on plots of observations in Fig. 7) of the vortex region: for 29 August–5 September, the progression of this orientation is ~40°E, 150°E, 240°E, 0°, 120°E, 200°E, 270°E, 300°E. Thus the motion of the vortex region has a period near 4 days (somewhat faster during the first 4 days and slower during the last 4). The overall shape and position of the vortex region (dark shading) are comparable in the observations and the transport calculations. In addition, on 3–5 September, when strong wave 1 amplification is occurring, tongues of high H_2O are seen to be drawn up around the vortex in both calculated and observed fields. These features appear increasingly patchy in the MLS observations at more equatorward latitudes due to sparser sampling there as the orbit tracks are farther apart. The transport calculations are also not expected to be as robust here because the assimilated winds used are less accurate in the Tropics and subtropics (e.g., Waugh 1996), where this material originated. Overall slightly higher H_2O in the transport calculations inside the vortex is consistent with the isentropic calculations since at this time and level diabatic descent is strongest inside the vortex; since vertical H_2O gradients are also relatively strong there (Fig. 2), lower H_2O is transported to this level by processes that were not included in the calculations. At this time and level, the 4-day wave is the strongest signal in the field; after this time, a more slowly moving wave 1 feature amplifies (e.g., Fig. 6; Fishbein et al. 1993). During the first 5–6 days shown in Fig. 7, when the 4-day wave is the dominant feature at this level, the entire vortex rotates with a period of ~4 days. At the end of this period (3–5 September), the 4-day wave is still present, although its amplitude is decreasing (Fig. 6); however, the amplifying slowly moving and quasi-stationary wave 1 features become dominant after ~5 September.

Plots of the wave 1 component filtered for 2.9–6.4-day periods for the last 4 days of the period shown in Fig. 7 (Fig. 8) show good agreement in both amplitude and phase at high latitudes (poleward of ~60°S), with the model showing a smaller phase shift near 60°S (e.g., see arrows on 3 September plot) than the observations. Poor agreement is seen near 50°S, where there is a sudden phase change in the observed 4-day wave that is much smaller in the transport calculations, and a larger 4-day wave amplitude in the transport calculations. Comparing the motion of the shaded region in Fig. 8 with the vortex position (dark shading) in Fig. 7 again demonstrates the significance of the 4-day wave in de-

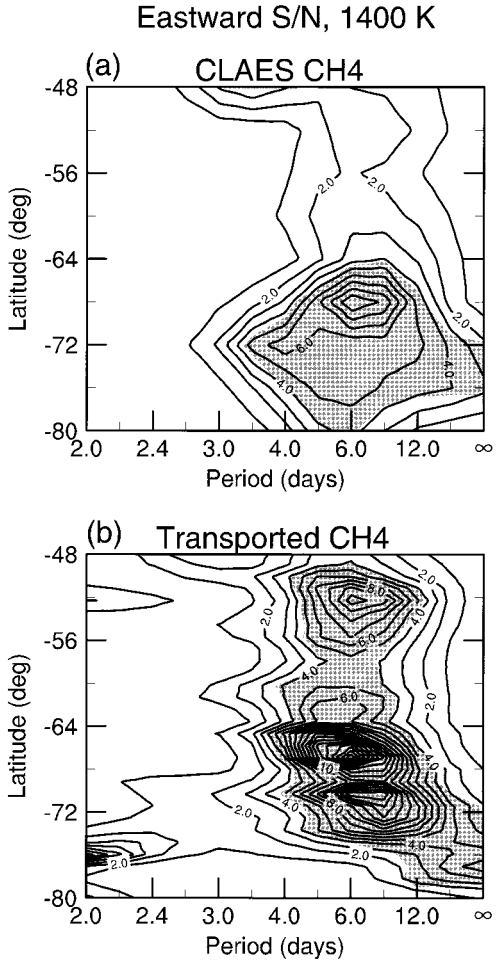

FIG. 9. ES/N at 1400 K for 24-day time series beginning on 17 Aug 1992 of (a) observed CLAES CH_4 and (b) CH_4 from a transport calculation initialized with CLAES CH_4 on 17 Aug 1992. Shading is as in Fig. 1.

termining the motion of the vortex at this level, as the indicated regions in Figs. 7 and 8 are nearly in phase and rotate at a similar rate.

c. Methane

Transport calculations for CH_4 were run at 1400 K and 1100 K, where zonal-mean CH_4 shows strong gradients at high latitudes (Fig. 2) and there were significant wave 1 signals at 72°S (Fig. 4). Figure 9 compares spectral analyses for observed and calculated CH_4 at 1400 K. Although, as for H_2O, agreement is poor near 50°S (with transport calculations showing a much stronger signal with a period ~8 day), both fields show signals with periods near 5–10 days at latitudes from about 76° to 60°S, a very slowly moving signal south of ~72°S, and a weak signal with ~4-day period near 70°S. Analyses of CH_4 and transported CH_4 at 1100 K show similar features, but with a stronger slowly moving wave 1 signal, and even weaker 4-day wave signal. Figure 10 shows Hovmöller plots of the complete wave 1 field in CH_4 at 1400 K and 72°S, and wave 1 filtered for 2.9–10.7-day periods, from observations and calculations. The strong slowly moving wave 1 signal that amplifies after about 2 September is apparent in both fields, with the same phase and approximately the same period, but ~20% larger amplitude in the transport calculations. The filtered plots in Fig. 10 show good agreement in the phase, time evolution, and amplitude of a wave with ~6-day period that reaches its maximum amplitude on ~4 September. When CLAES data are filtered for 3–6 days to isolate the (weak) 4-day wave signal, we find that the phase and amplitude of the 4-day wave agree well between calculations and observations, but the transported 4-day wave in CH_4 amplifies slightly later than the observed feature. As was the case with H_2O at 1800 K, spectral analyses and Hovmöller plots of PV at 1400 K show very similar signals to those in CH_4.

Figure 11 shows Hovmöller plots of wave 1 at 1100 K and 68°S in observed and transported CH_4. At this latitude and level, the small amplification of the slowly moving wave 1 near 25 August noted by Fishbein et al. (1993) is apparent in both observations and calculations, as well as the large wave 1 amplification event near 5 September. Figures 9, 10, and 11 all indicate a stronger stationary or very slowly moving wave 1 component in the transport calculations than in the observations.

Figure 12 shows a sequence of maps of CLAES CH_4 at 1400 K from observations and calculations for 2–5 September (the last 4 days shown for H_2O at 1800 K in Fig. 7, days chosen to be after those for which CLAES data were missing), showing good agreement in the shape and position of the vortex. Overall higher values for material that is drawn up around the vortex in the transport calculation are probably due to the absence of diabatic descent in that calculation since diabatic descent is strong at this time and tends to be strongest along the vortex edge on the side where material is being drawn up (e.g., Manney et al. 1994). Inspection of diabatic heating rates shows strong descent in the center of the vortex (where vertical CH_4 gradients are weak, as shown in Fig. 2) and outside the vortex on the side where high CH_4 is drawn up (where vertical CH_4 gradients are strong, as shown in Fig. 2). This pattern with greater differences between observations and calculations in the regions of high CH_4 probably contributes to the appearance of larger wave 1 amplitudes in the calculations. In contrast to the pattern at 1800 K in H_2O (Fig. 7), the vortex is larger at 1400 K and the rotation of the vortex itself has a long period, ~10–15 days. A faster rotation of material within the vortex can be seen in the maps from the transport calculations (and, albeit less clearly, in the observed maps) during the first 3 days shown here (see arrows). The slowly moving wave 1 is amplifying at the end of this period and becomes the dominant signal over all high latitudes.

Figure 13 shows similar maps of CH_4, but at 1100 K. The overall behavior is very similar to that at 1400

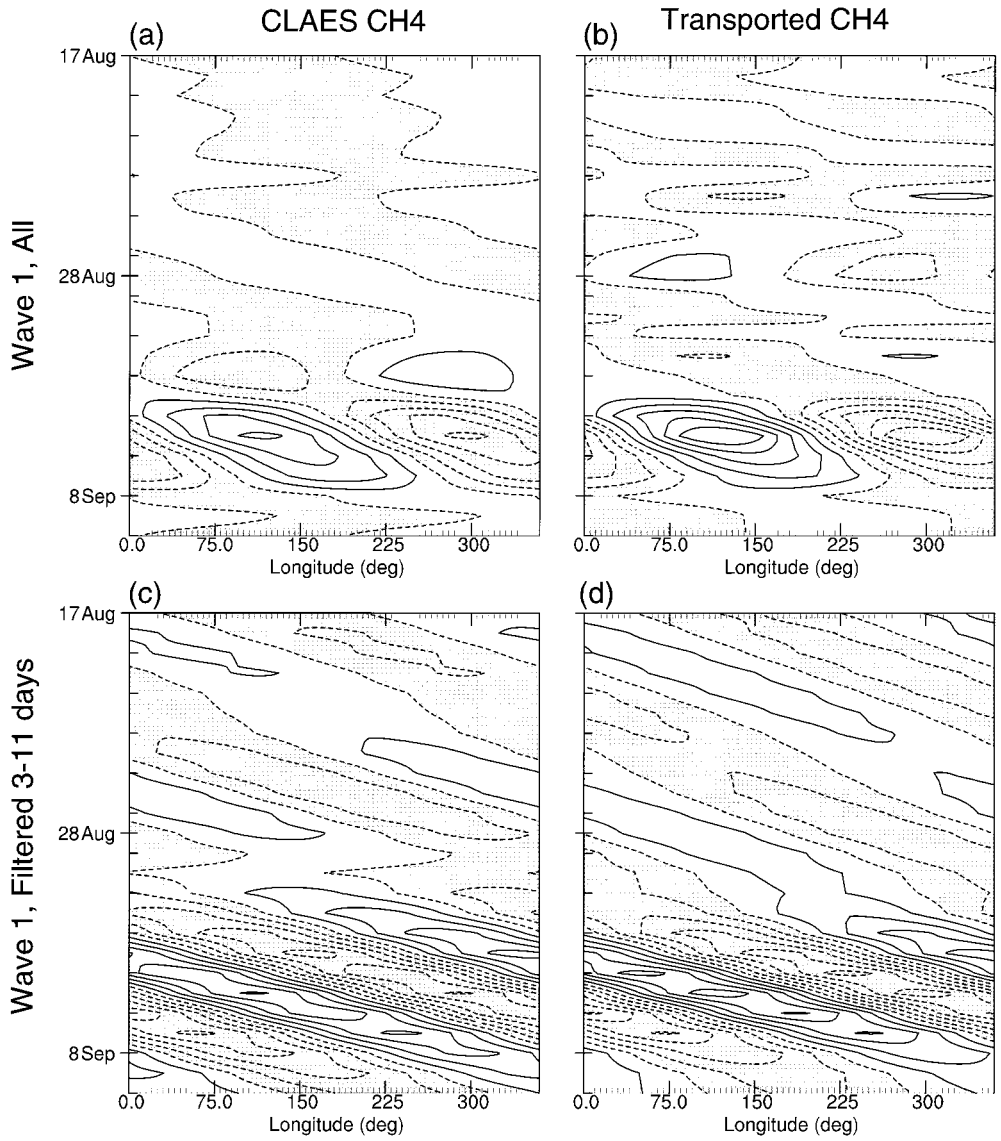

FIG. 10. Time–longitude (Hovmöller) plots at 1400 K and 72°S of wave 1 in CH_4 from (a) and (c) CLAES observations and (b) and (d) transport calculations, showing (a) and (b) total wave 1 field and (c) and (d) wave 1 filtered for 2.9–10.7-day periods. Contour interval on top is 0.036 ppmv, on bottom, 0.015 ppmv. Negative values are shaded.

K, with rapidly rotating material inside a more slowly moving vortex. The slowly moving wave 1 is weaker at this level on 2 September and builds up gradually. Comparison of Figs. 12 and 13 thus shows a westward and equatorward tilt of the vortex with height during the amplification of the slowly moving wave 1 feature. Comparison with Fig. 7 shows, most noticeably in the transport calculations on 2 and 3 September, that the smaller rapidly moving vortex at 1800 K is approximately in phase with the rapidly moving material in the inner vortex at the lower levels; that is, the 4-day wave during this period does not show any obvious phase tilt with height. As the slowly moving wave 1 amplifies (e.g., 3 September), we see the westward and equatorward tilt of the vortex extend up through 1800 K. At 1100 K, the intensification of the anticyclone discussed by Lahoz et al. (1996a) can be clearly seen, and the coiling of material in the anticyclone is apparent in the transport calculations. As noted by Lahoz et al. (1996a), this anticyclone progresses eastward, with the eastward progression slowing and its intensity decreasing as it reaches the date line.

d. Discussion

Because, as is apparent in Fig. 2, the structure of the tracers H_2O and CH_4 is such that a strong signal from transport by eastward moving waves is expected (and

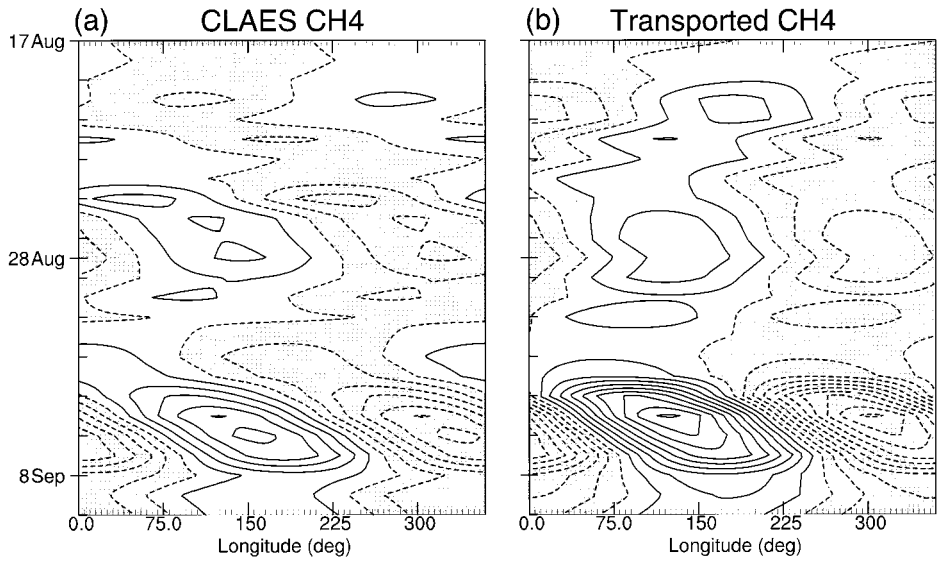

FIG. 11. Time–longitude (Hovmöller) plots at 1100 K and 68°S of wave 1 in CH_4 from (a) CLAES observations and (b) transport calculations. Contour interval is 0.04 ppmv. Negative values are shaded.

appears, Fig. 4) only over a limited range of levels, it is somewhat difficult to get a clear picture of the three-dimensional structure of the wave motions. To clarify this, we look at the observed evolution of UKMO PV; as noted above, spectral analyses of PV and transported PV tracer show very similar signals to those of H_2O and CH_4, but since PV has strong horizontal gradients over the entire range of altitudes shown, all of the features discussed above can be seen in PV. We show the three-dimensional evolution of the wave features by presenting fields of PV scaled in ''vorticity units'' (e.g., Dunkerton and Delisi 1986), as described in detail by Manney et al. (1994), so as to have a similar range of values at all levels. Figure 14 shows a 6-day sequence of the departure of scaled PV from the zonal mean, as a function of potential temperature, around the 72°S latitude circle, with the wave 1 component of this eddy indicated in the background. As can be seen from Figs. 7, 12, and 13, this cuts through the vortex edge at the highest levels shown and through the inner vortex material at the lower levels. An approximately 4-day motion of wave 1 at all levels above ~1000 K in the first

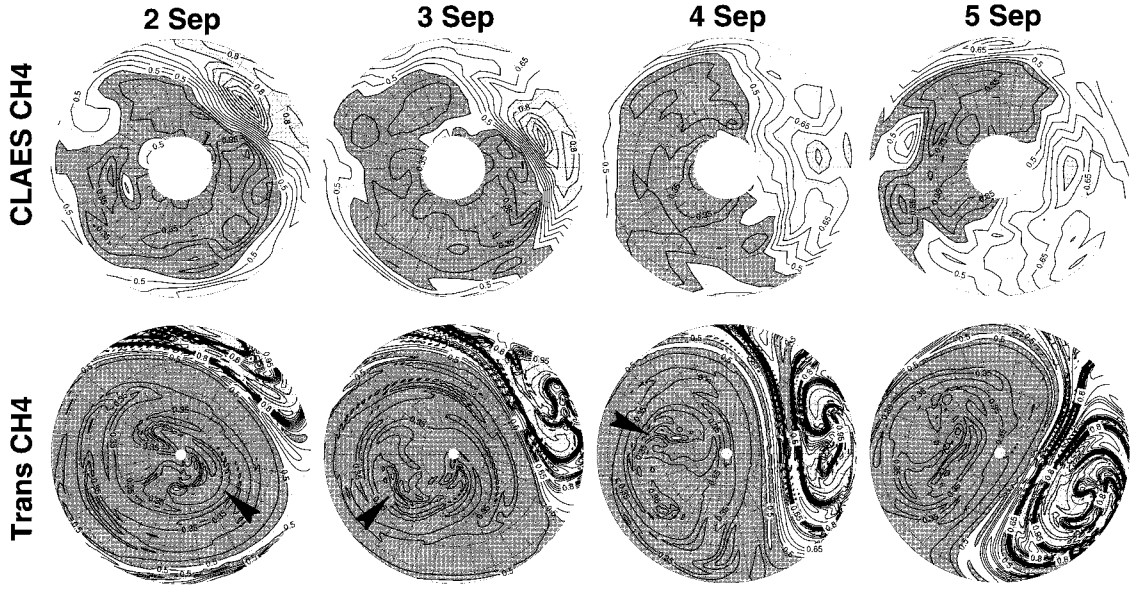

FIG. 12. Maps of CH_4 (ppmv) at 1400 K for 2–5 Sep 1992 from CLAES observations (top) and transport calculations (bottom). Layout is as in Fig. 7. Contour interval is 0.05 ppmv, with dark shading from 0.2 to 0.45 ppmv and light shading from 0.75 to 1.3 ppmv.

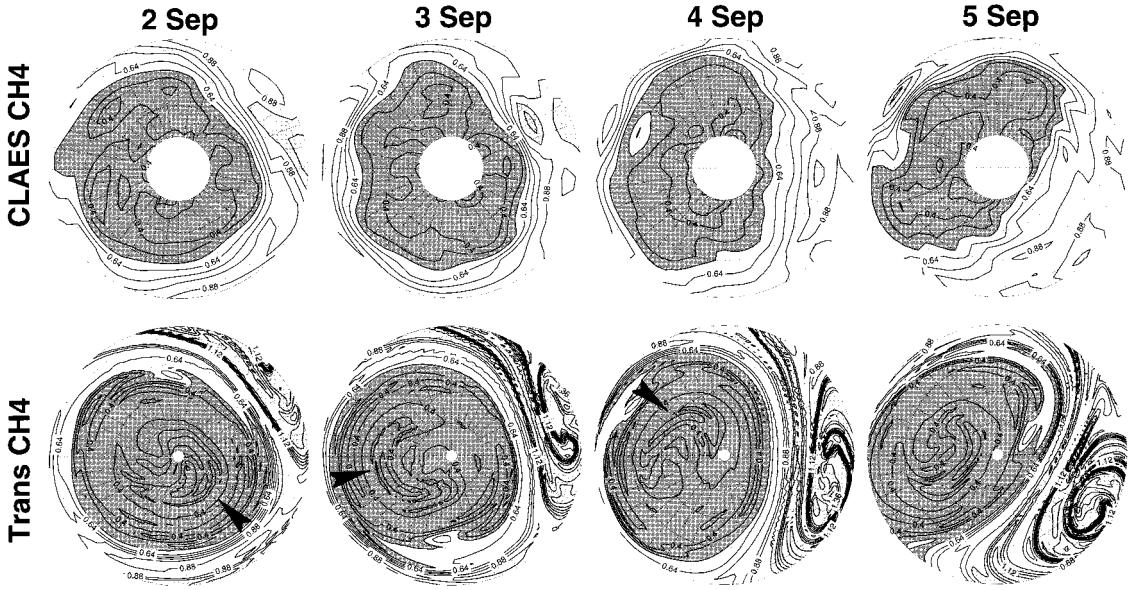

FIG. 13. As in Fig. 12, but at 1100 K. Contour interval is 0.08 ppmv, with dark shading from 0.2 to 0.56 ppmv and light shading from 0.96 to 1.6 ppmv.

5 days shown is evident in the regular eastward motion of the medium-shaded region such that it rotates to its initial position by 1 September. That this motion is the dominant signal at the highest levels at the end of August can be seen by comparing the wave 1 and full eddy fields (although there are significant features at higher wavenumbers) in that the strongest region of positive anomaly remains in phase with this wave 1. At the lowest levels shown, a slowly moving or stationary wave 1 is dominant throughout the period; this feature only becomes obvious at the highest levels in the last few days shown.

Figure 15 shows an isosurface of PV that is toward the inner part of the region of strong PV gradients de-

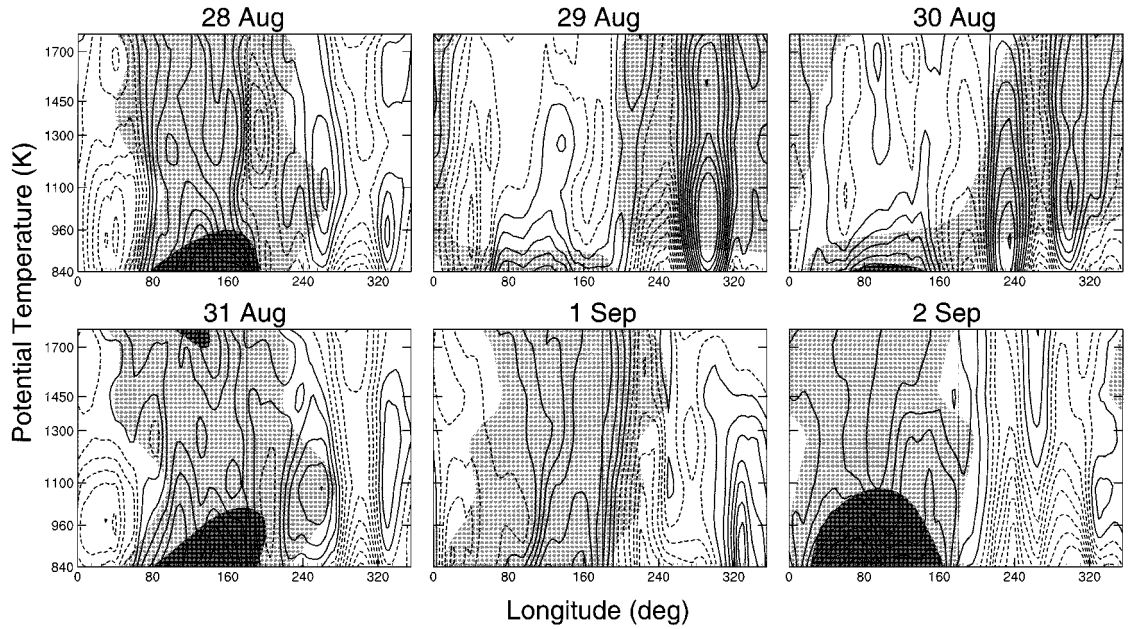

FIG. 14. Cross sections as a function of potential temperature around 72°S of the departure of scaled PV (calculated from UKMO data) from the zonal mean (contours), for 28 Aug–2 Sep 1992. Contour interval is 0.1×10^{-4} s^{-1}; dashed lines indicate negative values. In the background is the wave 1 component of the eddy, with a 0.25×10^{-4} s^{-1} contour interval, and light gray and white representing negative values.

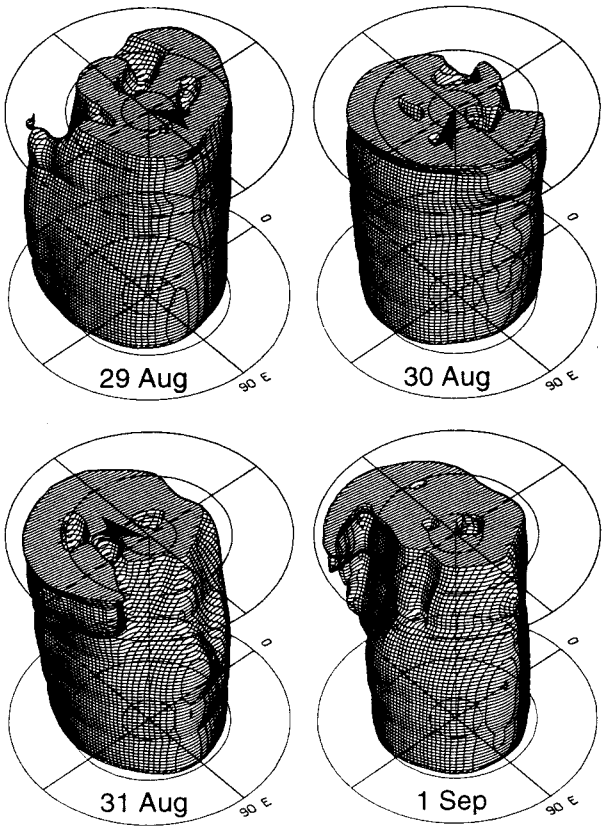

FIG. 15. Time sequence of an isosurface of UKMO PV representative of the polar vortex edge for 29 Aug–1 Sep 1992, shown from 840 to 1800 K. A contour representative of the vortex edge at all levels was obtained by scaling at each level so that the region of strong gradients (during this particular time period) was at approximately the same numerical value. Zonal wavenumbers greater than six were filtered out of the PV fields before plotting.

marking the vortex edge, showing approximately the evolution of the vortex. As was apparent in H_2O in Fig. 7, during the first 3 days shown here the entire vortex at the top [which has already been eroded at these levels and is thus smaller and weaker than in midwinter—as is typical in the Southern Hemisphere the final warming and vortex breakup proceeds from the top down (e.g., Manney et al. 1994; Lahoz et al. 1996a)] rotates with a 4-day period (indicated roughly by the arrows), whereas at the lower levels it is nearly stationary. On 31 August and 1 September, a large tail splits off the inner part of the vortex at the highest levels, as a slowly moving anticyclone begins to develop (Lahoz et al. 1996a); this tail moves slowly eastward, and tends to mask the 4-day motion of the rest of the vortex after this time.

Fishbein et al. (1993) showed ~10-day and quasi-stationary wave 1 features interfering constructively near 25 August and 5 September, leading to a small amplification of wave 1 around 25 August and a large amplification around 5 September. The first of these events can been seen in Hovmöller plots of CH_4 at 1100 K (Fig. 11). The large wave 1 amplification around 5 September is seen throughout the stratosphere. At 1800 K, the 4-day wave existed prior to the first of these amplifications (Fig. 6) and comprises at least four cycles. The 4-day rotation around the pole appears clearly before about 1 September and is not masked by the displacement of the vortex off the pole due to slowly moving waves associated with anticyclogenesis (Figs. 6, 7, 14, and 15). The large wave 1 amplification near 5 September is linked to the genesis of a strong anticyclone, as shown by Lahoz et al. (1996a). By about 3 September, this anticyclone spans the range of levels studied; it propagates slowly eastward (Figs. 7, 12, and 13), becoming stationary and weakening somewhat as it reaches the date line (Figs. 6, 10, and 11; Lahoz et al. 1996a).

The behavior of PV shown in Figs. 14 and 15 demonstrates more clearly the evolution that is apparent in the tracers H_2O and CH_4. At the highest levels studied, where the late winter vortex has been somewhat eroded, the entire vortex rotates with a 4-day period at the time of maximum 4-day wave amplitude, whereas at lower levels, the 4-day motion is confined within the vortex. Bowman and Chen (1994) and Orsolini and Simon (1995) found, in idealized studies of transport by barotropically unstable waves like the 4-day wave, that mixing by these waves was in general confined inside the polar vortex. Their results appear qualitatively similar to the situation we have seen at the lower levels. Since their simulations were for strong, midwinter-like vortices, our results from observations and transport calculations using observed winds appear to confirm those results showing that the effects of transport by the 4-day wave were confined within the vortex. In contrast, we have seen that at 1800 K the entire vortex rotates with a 4-day period, and further examination of observed and transported H_2O maps such as those in Fig. 7 indicates that during the time when the 4-day wave is dominant, material is being drawn off the vortex edge and mixed into midlatitudes. This type of behavior has not been seen in idealized simulations [although Orsolini and Simon (1995) showed some mixing between the vortex and its edge during wave decay]. This is probably because situations with a small and somewhat weakened vortex such as that at 1800 K in late austral winter 1992 have not been examined. In addition, the observed and simulated behavior shown here, in the presence of other wave features, exhibits a degree of complexity that would not be expected in simulations of the 4-day wave in isolation.

The 4-day wave is generally thought to originate via instability (e.g., Manney and Randel 1993, and references therein), in many cases primarily barotropic instability. Allen et al. (1997) showed that the necessary conditions for instability were indeed fulfilled during the time period studied here. Their results, the confinement of the 4-day wave to the upper stratosphere and lower mesosphere (as noted in previous studies), and

the lack of phase tilt with height of the 4-day wave in the upper stratosphere shown here suggest that in this period the mechanism may be primarily barotropic instability. However, as shown above, the observed situation is never that of a simple unstable wave growing on a zonally symmetric basic state. As well as the slowly moving and quasi-stationary wave 1 features discussed above, a relatively strong, slowly eastward moving wave 2 amplified around 23 August and 3 September (although its amplitude was never over about half the maximum reached by wave 1); this type of wave 2 feature is common in the austral late winter and spring (e.g., Manney et al. 1991). Manney et al. (1989) showed that the presence of waves resembling those typically observed in the stratosphere could have a marked effect on the stability of the stratospheric polar night jet. In particular, they found that, although a slowly moving or stationary wave 1 did not materially affect the stability of modes resembling the 4-day wave, a slowly eastward moving wave 2 of very modest amplitude could, in fact, considerably destabilize such modes. They also found that if a mode resembling the 4-day wave was already present, it could lead to further amplification of quasi-nondispersive features moving with the same phase speeds. We can see (Figs. 6 and 10) that the 4-day wave amplified earlier at higher altitudes; resonant-type behavior such as that found in the theoretical studies of Manney et al. (1989) could contribute to the subsequent amplification at lower altitudes. Because of the variety of wave activity present during August and September 1992, such considerations are undoubtedly important in determining the observed life cycle of the 4-day wave.

4. Summary

We have examined *UARS* tracer data and isentropic transport calculations initialized with these data for evidence of eastward-traveling waves in the polar upper stratosphere in late Austral winter 1992. Spectral analyses of MLS H_2O from prototype iterative retrievals indicate a 4-day wave signal in H_2O, at levels ~1.5–0.1 hPa. At levels below ~1.5 hPa, horizontal H_2O gradients are weak in high latitudes, so a signal that is produced mainly by horizontal transport would not be expected. The 4-day wave in H_2O at 1800 K (~1–1.5 hPa) has a double-peaked structure in latitude, with maximum amplitudes near 72°S and 60°S. A 4-day wave signal was not obvious in production retrievals of MLS H_2O, due to deficiencies in those retrievals. Isentropic transport calculations initialized with MLS H_2O reproduce a double-peaked structure, with maxima at approximately the same latitudes. The time evolution, amplitude, and phase of the 4-day wave in the transport calculations agree well with those in observations at high latitudes. Near 50°S, the observations show a sudden phase change, that is much larger than that in the calculations, and the calculations show a larger 4-day wave signal. Qualitative agreement between the full H_2O fields in calculations and observations at 1800 K is good at high latitudes (poleward of ~60°S), with the position and shape of the polar vortex reproduced by the calculations; the calculations also show tongues of higher H_2O drawn up around the vortex when wave 1 amplifies, qualitatively similar to features seen in the data.

CLAES CH_4 observations show strong horizontal gradients at high latitudes below ~2 hPa, and spectral analysis of CH_4 shows eastward-traveling wave features with periods of 5–12 days below ~2 hPa and a weak 4-day wave feature between ~4 and 2 hPa. Transport calculations initialized with CH_4 show similar eastward-traveling signals, with good agreement between the phase of observed and calculated fields at high latitudes. The transport calculations show a stronger stationary component than the observed CH_4, and, as in H_2O, disagreement at lower latitudes where fast-moving wave amplitudes are small. There is overall qualitative agreement of the position of the vortex and of tongues of high CH_4 drawn up around the vortex in observed and transported fields.

Several factors may influence the lack of quantitative agreement between observations and calculations. Diabatic descent rates are relatively large in the polar middle and upper stratosphere at this time, so the inclusion of only horizontal motions in the transport calculations leads us to expect some differences. Also, the coarse horizontal resolution of the observed fields leads to differences in detail, as small or narrow features seen in the transport calculations, even if they were present in the real atmosphere, might be missed or misrepresented by the sampling pattern of the satellite instruments. Different relatively small scale features will be sampled by the satellite instruments on different days, depending on their location with respect to the sampling pattern; thus, the MLS and CLAES initialization fields may include some, but not all, of the relatively small scale structure that is present in the atmosphere. Finally, in any transport calculation, the accuracy of the advecting winds is problematic and difficult to assess quantitatively. Some previous transport calculations using UKMO winds show agreement between observed and calculated tracers that is relatively poor in midlatitudes (outside the vortex, away from its edge) (e.g., Manney et al. 1995). Both observations (due to denser sampling) and model calculations (due to better wind quality) are thus expected to be more reliable at the high latitudes we have focused on here.

Despite some points of disagreement between observed and calculated fields, the transport calculations were successful in qualitatively reproducing the phase and time evolution of high-latitude eastward-traveling waves in the polar upper stratosphere in late southern winter 1992. This success indicates that the UKMO winds used for the transport calculations are generally reliable in this region, and that the eastward-traveling

wave features identified in the MLS H_2O and CLAES CH_4 originate to a large extent from horizontal transport processes.

The observed and transported tracer fields at the various levels studied show three-dimensional evolution of the 4-day wave in relation to the polar vortex that is consistent with the evolution of PV at this time. At the highest levels, near 1800 K, the vortex is small and weakened in late winter, and the entire vortex rotates with a 4-day period at the peak of the 4-day wave amplitude; at 1800 K, material is drawn off the vortex edge and mixed into midlatitudes during this period, suggesting that the 4-day wave in this situation is a significant factor in vortex/extravortex mixing. At lower levels (~1400 K and below), the 4-day rotation is confined to material in the inner part of a large, strong vortex, which rotates with a much slower period.

Acknowledgments. Thanks to the MLS and CLAES teams for their efforts in making the data available, the UKMO (R. Swinbank, A. O'Neill) for meteorological data, Drs. L. S. Elson and R. P. Thurstans for asynoptic mapping of MLS and CLAES data, Dr. M. L. Santee for CLAES data examination and helpful discussions, and Drs. D. R. Allen, W. A. Lahoz, and three anonymous reviewers for helpful comments on the original manuscript. Part of this work was carried out while Y. J. Orsolini was a visiting scientist at Centre National de Recherches Météorologiques. Work at the University of Edinburgh (H. C. Pumphrey) was supported by the Natural Environment Research Council (NERC). Work at the Jet Propulsion Laboratory, California Institute of Technology and at the Lockheed Martin Palo Alto Laboratory was done under contract with the National Aeronautics and Space Administration.

REFERENCES

Allen, D. R., J. L. Stanford, L. S. Elson, E. F. Fishbein, L. Froidevaux, and J. W. Waters, 1997: The 4-day wave as observed from the *Upper Atmosphere Research Satellite* Microwave Limb Sounder. *J. Atmos. Sci.,* **54,** 420–434.

Bowman, K. P., and P. Chen, 1994: Mixing by barotropic instability in a nonlinear model. *J. Atmos. Sci.,* **51,** 3692–3705.

Brasseur, G., and S. Solomon, 1986: *Aeronomy of the Middle Atmosphere*. 2d ed., Reidel, 441 pp.

Dunkerton, T. J., and D. P. Delisi, 1986: Evolution of potential vorticity in the winter stratosphere of January–February 1979. *J. Geophys. Res.,* **91,** 1199–1208.

Elson, L. S., and L. Froidevaux, 1993: The use of Fourier transforms for asynoptic mapping: Early results from the Upper Atmosphere Research Satellite Microwave Limb Sounder. *J. Geophys. Res.,* **98,** 23 039–23 049.

Fishbein, E. F., L. S. Elson. L. Froidevaux, G. L. Manney, W. G. Read, J. W. Waters, and R. W. Zurek, 1993: MLS observations of stratospheric waves in temperature and ozone during the 1992 southern winter. *Geophys. Res. Lett.,* **20,** 1255–1258.

Hartmann, D. L., and R. R. Garcia, 1979: A mechanistic model of ozone transport by planetary waves in the stratosphere. *J. Atmos. Sci.,* **36,** 350–364.

Lahoz, W. A., A. O'Neill, A. Heaps, V. D. Pope, R. Swinbank, R. S. Harwood, L. Froidevaux, W. G. Read, J. W. Waters, and G. E. Peckham, 1996a: Vortex dynamics and the evolution of water vapour in the stratosphere of the Southern Hemisphere. *Quart. J. Roy. Meteor. Soc.,* **122,** 423–450.

——, and Coauthors 1996b: Validation of UARS Microwave Limb Sounder 183 GHz H_2O measurements. *J. Geophys. Res.,* **101,** 10 129–10 149.

Lary, D. J., M. P. Chipperfield, J. A. Pyle, W. A. Norton, and L. P. Riishojgaard, 1995: Three-dimensional tracer initialization and general diagnostics using equivalent PV latitude-potential-temperature coordinates. *Quart. J. Roy. Meteor. Soc.,* **121,** 187–210.

Manney, G. L., 1991: The stratospheric 4-day wave in NMC data. *J. Atmos. Sci.,* **48,** 1798–1811.

——, and W. J. Randel, 1993: Instability at the winter stratopause: A mechanism for the 4-day wave. *J. Atmos. Sci.,* **50,** 3928–2938.

——, T. R. Nathan, and J. L. Stanford, 1989: Barotropic instability of basic states with a realistic jet and a wave. *J. Atmos. Sci.,* **46,** 1250–1273.

——, J. D. Farrara, and C. R. Mechoso, 1991: The behavior of wave 2 in the Southern Hemisphere stratosphere during late winter and early spring. *J. Atmos. Sci.,* **48,** 976–998.

——, R. W. Zurek, A. O'Neill, and R. Swinbank, 1994: On the motion of air through the stratospheric polar vortex. *J. Atmos. Sci.,* **51,** 2973–2994.

——, ——, W. A. Lahoz, R. S. Harwood, J. C. Gille, J. B. Kumer, J. L. Mergenthaler, A. E. Roche, A. O'Neill, R. Swinbank, and J. W. Waters, 1995: Lagrangian transport calculations using *UARS* data. Part I: Passive tracers. *J. Atmos. Sci.,* **52,** 3049–3068.

Orsolini, Y. J., 1995: On the formation of ozone laminae at the edge of the Arctic polar vortex. *Quart. J. Roy. Meteor. Soc.,* **121,** 1923–1941.

——, and P. Simon, 1995: Idealized life cycles of planetary-scale barotropic waves in the middle atmosphere. *J. Atmos. Sci.,* **52,** 3817–3835.

——, G. Hansen, U.-P. Hoppe, G. L. Manney, and K. H. Fricke, 1997: Dynamical modelling of wintertime Lidar observations in the Arctic: Ozone laminae, and ozone depletion. *Quart. J. Roy. Meteor. Soc.,* **123,** 785–800.

Pumphrey, H. C., 1998: Nonlinear retrievals of water vapour from the UARS Microwave Limb Sounder (MLS). *Adv. Space Res.,* **21,** 389–392.

Randel, W. J., and L. R. Lait, 1991: Dynamics of the 4-day wave in the Southern Hemisphere polar stratosphere. *J. Atmos. Sci.,* **48,** 2496–2508.

Roche, A. E., and Coauthors, 1996: Validation of CH_4 and N_2O measurements by the Cryogen Limb Array Etalon Spectrometer instrument on the Upper Atmosphere Research Satellite. *J. Geophys. Res.,* **101,** 9679–9710.

Swinbank, R., and A. O'Neill, 1994: A stratosphere–troposphere data assimilation system. *Mon. Wea. Rev.,* **122,** 686–702.

Venne, D. E., and J. L. Stanford, 1982: An observational study of high-latitude stratospheric planetary waves in winter. *J. Atmos. Sci.,* **39,** 1026–1034.

Waugh, D. W., 1996: Seasonal variation of isentropic transport out of the tropical stratosphere, *J. Geophys. Res.,* **101,** 4007–4023.